Application of He I Line Intensity Ratio Method to Lyot-Filter-Based Imaging Spectrometry on MAP-II Divertor Simulator*)

Shinichiro KADO

Institute of Advanced Energy, Kyoto University, Uji 611-0011, Japan

(Received 3 October 2018 / Accepted 2 July 2019)

A simple, yet advanced technique of imaging spectrometry of divertor-relevant low-temperature plasmas using a wavelength-tunable Lyot filter spectral camera is herein proposed. The influence of the radiation-trapping effect in the atomic helium line intensity ratio method, characterized by the trapping radius, L_q, can be reduced using only the triplet series: 471(4^3S)-, 587(3^3D)-, and 706(3^3S)-nm lines that are included in the tunable range of the above-mentioned Lyot filter. Approximate values of L_q can be estimated by adding 501(3^1P)- and 667(3^1D)-nm singlet lines, which enables stand-alone parameter imaging considering the radiation trapping.

Keywords: Lyot filter, imaging spectroscopy, line intensity ratio, atomic helium line, leak band, collisional-radiative model, radiation trapping

DOI: 10.1585/pfr.14.2402140

1. Introduction

Spectral line intensity ratios [1], in combination with a collisional-radiative (CR) model [2] of atomic helium, have widely been applied to the measurement of the electron temperature T_e and electron density n_e in divertor/edge plasma of fusion reactor and linear divertor simulators. Because the plasma parameters have a spatial distribution, the need to applying this method to imaging spectrometry, in particular, is increasing.

To meet this need, we have developed an imaging spectrometry using a spectral camera. It comprises a wavelength-tunable bandpass filter, known as a "Lyot filter," and a two-dimensional imaging detector [3, 4]. The Lyot filter is a type of birefringent filter based on polarization interference between multistage optical units. The wavelength tunability is achieved by varying the retardance of the nematic liquid crystals in each unit. The product adopted in this study has a tunable range of 400 - 720 nm. This implies that the widely used He I line of 728 nm (2^1P – 3^1S) cannot be utilized in this technique.

Additionally, it is to be noted that the leak-band problem associated with Lyot filters has already been identified in previous works [3, 4]. At a certain wavelength tuning of shorter than 455 nm, a photon at a different wavelength longer than approximately 548 nm was found to be transmitted, similar to an interference fringe, which disturbs the quantitative calibration and measurements.

In the present work, practical combinations of spectral lines of atomic helium in the leak-band free wavelength and without 728 nm line are proposed for Lyot filter imaging spectrometry of divertor-relevant low-temperature plasmas where radiation trapping influences the population distribution. Experiments were conducted for low-temperature helium plasmas produced in the MAP-II (material and plasma) linear divertor simulator [5], which was moved from the University of Tokyo to Tsukuba University in 2014.

2. Line Selection in He I CR Model for Lyot Filter Camera

The degree of radiation trapping can be characterized by the equivalent trapping radius, L_q, in the Otsuka–Iida formula [6] for the optical escape factor (OEF), Λ, in the center of the uniform radiation field having the dimension of L_q, *i.e.*, uniform upper-state population, as a function of the optical depth, τ,

$$\Lambda(\tau) = \min\left(1, \frac{3.811 - 3.284\left(1 + (a\tau)^b\right)^{-1}}{(a\tau + 0.429)\left(\pi \ln(b + a\tau)\right)^{0.675}}\right), \tag{1}$$

$$\tau \propto f_{pq}\lambda_{qp}\sqrt{\frac{M}{k_B T_p}} n_p L_q, \tag{2}$$

where $a = 2.658$, and $b = 1.499$. The subscripts q and p represent the upper and lower states of the transition, respectively. τ is proportional to the oscillator strength f, transition wavelength λ, the reciprocal of the thermal velocity of the lower-state particle (where M, T_p, and k_B denote the atomic mass, atomic temperature, and Boltzmann constant, respectively), the lower-state population n_p, and

author's e-mail: kado@iae.kyoto-u.ac.jp

*) This article is based on the presentation at the 12th International Conference on Open Magnetic Systems for Plasma Confinement (OS2018).

L_q.

The OEF, in reality, depends on the spatial profile of the upper-state population applied in the calculation model. There are, in fact, various kinds of radiation-trapping models, and, in all cases, a certain assumption of the shapes of the radiation field, *i.e.*, the upper-state population, is made. Consequently, the resultant escape factor *can be* different. As discussed in previous work [7], however, one can adjust L_q to yield an equivalent escape factor. This seemingly arbitral assumption is occasionally referred to as "similarity of OEF with respect to tau," and L_q is referred to as an "effective-L." In other words, if we consider that L_q is not necessarily the real distance but can be a virtual length having the unit of length, determination of L_q is equivalent to the synthetic determination of Λ or τ through experiments. This consideration simplifies the treatment of radiation trapping to a significant extent, except for an extreme case in which, for instance, the local Λ exhibits a negative value. A detailed discussion of the above-mentioned matter is provided in Refs. [6, 7].

Effective-L, the degree of the radiation-trapping effect in the collisional-radiative model calculation [8], can be determined using several methods, regardless of what it is called [9,10]. We had presented in Refs. [6,11] the usage of the population ratio of $n(3^1\mathrm{P};\ 501\,\mathrm{nm})/n(4^1\mathrm{P};\ 396\,\mathrm{nm})$ combined with the n_e measurement using a Langmuir probe ($3^1\mathrm{P}/4^1\mathrm{P}$ method, hereafter). The ratio is insensitive to T_e at 2 - 8 eV, while highly sensitive to n_e and L_q. Therefore, if n_e is determined, say, using the Langmuir probe, L_q can be specified.

Application of the effective-L principle in imaging spectrometry, however, encounters the problem of how to measure the image of the electron density. Because it is desirable to determine n_e and T_e only from the spectroscopic data, the sensitivity of a typical population ratio to the value of L_q was herein investigated.

Figure 1 illustrates the contour plot of the population ratios of He I as a function of n_e and T_e calculated based on the collisional-radiative model. The wavelength that directly corresponds to the upper state of the radiative decay to the principal quantum number $n = 2$ states is provided in parentheses. Figure 1 (a) depicts the group of three lines, 471(4^3S), 587(3^3D), and 706(3^3S) nm, that was found to be less sensitive to the choice of L_q, even though *some* approximate value was necessary. Figure 1 (b), on the other hand, depicts another group of three lines, 471(4^3S), 501(3^1P), and 667(3^1D) nm, which is highly sensitive to L_q. The reason for this difference can be described as follows. The 3^1P state is a resonance level strongly coupled to the ground level optically. Accordingly, the 3^1D state population is influenced by the redistribution from the ^{1}P states through the collisional-radiative processes. However, the population ratio among the triplet states is less affected by the radiation trapping occurring in the singlet states. The effect of radiation trapping is different in different states, so that 3^1P and 4^1P undergo different OEFs. This implies that

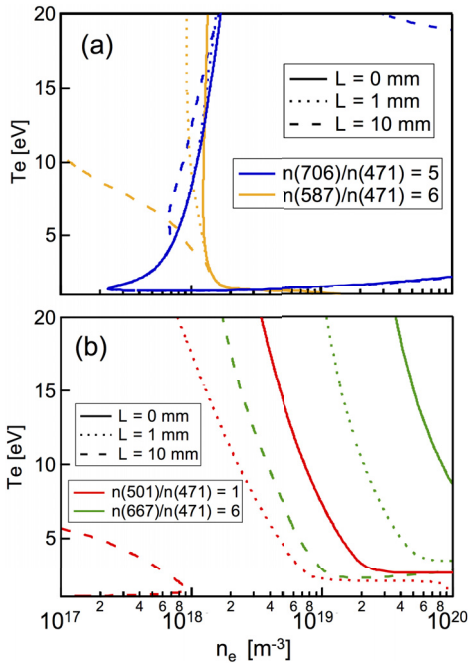

Fig. 1 L_p (= L) dependence of the population ratio: (a) $n(3^3\mathrm{S};\ 706\,\mathrm{nm})/n(4^3\mathrm{S};\ 471\,\mathrm{nm})$ and $n(3^3\mathrm{D};\ 587\,\mathrm{nm})/n(4^3\mathrm{S};\ 471\,\mathrm{nm})$, and (b) $n(3^1\mathrm{P};\ 501\,\mathrm{nm})/n(4^3\mathrm{S};\ 471\,\mathrm{nm})$ and $n(3^1\mathrm{D};\ 667\,\mathrm{nm})/n(4^3\mathrm{S};\ 471\,\mathrm{nm})$ — pressure 10 mTorr.

more lines are necessary to reproduce the synthetic spectra. In fact, a previous study [9] measured 16 lines for the determination of n_e, T_e, radiation trapping, and metastable density. In the present case, reducing the number of lines was preferred, because only one image could be recorded for the tuned wavelength. Therefore, the single value of L_q was represented for all the states to which OEF was applied.

In this respect, two strategies can be proposed:
(i) Using *three lines* of 471(4^3S), 587(3^3D), and 706(3^3S) nm whose ratio is robust against the assumption of the degree of radiation trapping, characterized by the equivalent trapping radius in the Otsuka–Iida formula [6], and
(ii) Adding two more lines of 501(3^1P) and 667(3^1D) nm, namely, using *five lines* and determining the trapping radius L_q, as well as T_e and n_e. Note that 396(4^1P) nm line is out of the range of the Lyot filter.

The synthetic plasma parameter determination was based on the downhill simplex method to minimize the evaluation function of the difference between the calculated and measured population ratios. Generally, three-parameter (n_e, T_e, L_q) determination needed a much longer time to converge than the in the case of two-parameter (n_e, T_e).

The sensitivity of $n(3^3\mathrm{D};\ 587\,\mathrm{nm})/n(4^3\mathrm{S};\ 471\,\mathrm{nm})$ to L_q increased if this value was over several millimeters. In this situation, for example, it is necessary to accept the uncertainty of about a few tens of percent in n_e measurement in the three-line strategy. This suggests that if these popu-

lation ratios are used, one can determine n_e and T_e without the knowledge of the precise value of L_q.

3. Proof-of Principle Experiments

3.1 Experimental setup

MAP-II [5] consists of a dual-chamber approximately 500 mm in diameter and 500 mm in length connected by means of a drift tube between the chambers. A longitudinal magnetic field of about 20 mT is applied. The diameter of the plasma column is about 25 mm in half width at half maximum. The helium working gas pressure varied from 2.1 to 25.3 mTorr. In this study, the results for 5.0 and 8.0 mTorr were chosen as typical conditions (shot# 26240 and 26237, respectively).

The Lyot filter spectral camera is located at an observation window of the downstream chamber. The tunable Lyot filter (CRI Inc., Varispec, VIS-7-20), covering the 400-720-nm region, 7 nm in typical pass-band and about 12% in nonpolarized light transmittance at 550-nm and 20-mm diameter, is attached to the front side of the photographic lens (Nikon), 24 mm in focal length and 2.8 in f-number. However, the iris for the measurement is set to $f/11$, since the area of the cooled charge-coupled device (CCD) detector (Roper, EEV 1024 × 256 pixels, 26 μm in each pixel size) that is free from vignetting becomes larger for a smaller aperture. The observable range of this optical system is 199×140 mm^2, as shown in Fig. 2 (a). Although the pixel-based precise Abel inversion from the spectral image was possible in principle, the measured image was smoothened by the curve-fitting procedure to eliminate the noise component.

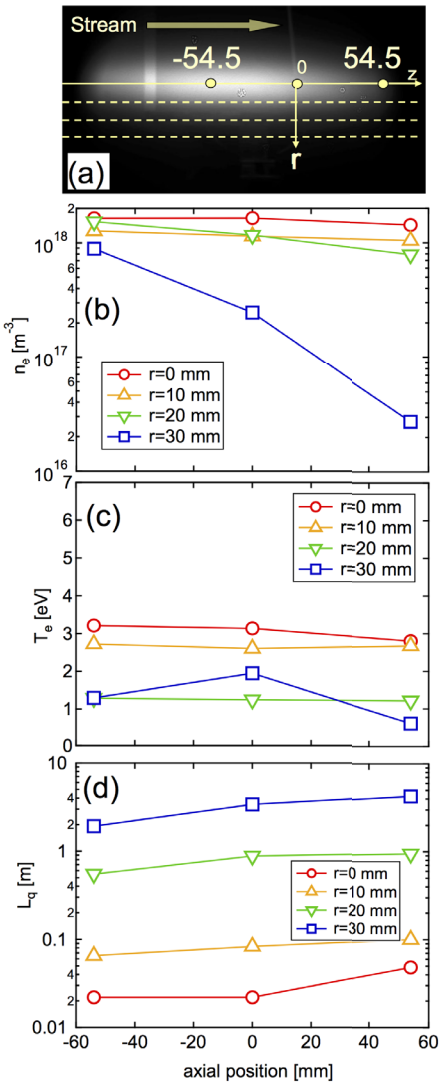

Fig. 2 (a) Side view of the imaging measurement of the plasma stream (b) n_e, (c) T_e, and (d) L_q determined from the five-line method [shot#26240, 5 mTorr].

3.2 Axial profile from parameter imaging

Since the Langmuir probe was fixed at the axial position $z = 0$, the five-line method(ii) that is independent of the probe measurement was utilized for several selected positions to determine three parameters (n_e, T_e, L_q) simultaneously, as shown in Figs. 2(b-d). From each horizontal plane separated vertically by a distance of 10 mm, three axial positions were picked up in the detector at a distance of $z = 0$ and $+/-54.5$ mm. The determined L_q were different at each position, suggesting that the radiation-trapping effect had a spatial dependence. This also suggests that evaluation of L_q using the $3^1P/4^1P$ method cannot be applied to imaging spectrometry directly. Therefore, a practical solution is proposed in the following subsection.

3.3 Radial profile from parameter imaging

Radial profiles of n_e and T_e at $z = 0$ determined by

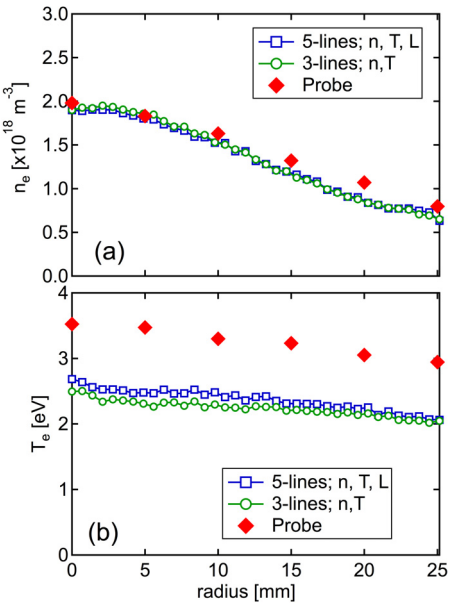

Fig. 3 Comparison of n_e and T_e obtained from three-line and five-line methods with those obtained using the Langmuir probe [#26237, 8 mTorr].

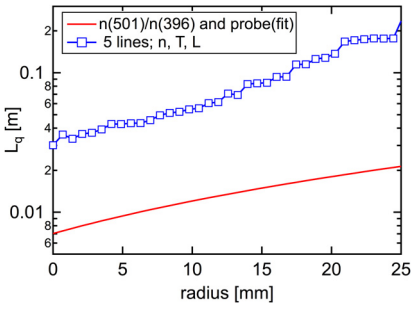

Fig. 4 Comparison of L_p obtained from five-line methods with those by the $n(501;\ 3^1P)/n(396;\ 4^1P)$ ratio combined with the Langmuir probe [#26237, 8 mTorr].

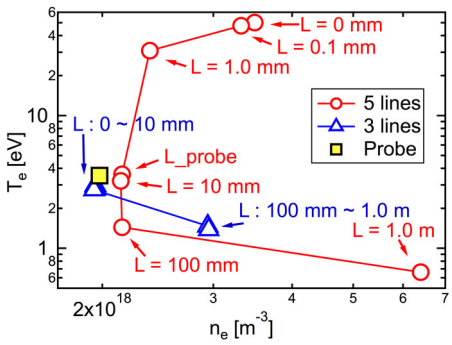

Fig. 5 Sensitivity of the synthesized to the approximated values of L_p: Data were adopted by the central position for shot#26237 (8 mTorr) — L_probe = 7.02 mm determined from the $3^1P/4^1P$ method.

the three- and five-line methods are shown in Fig. 3. In the three-line method, the value of L_q determined by the five-line method was adopted. The parameters measured by the Langmuir probe are plotted for comparison. Both n_e and T_e were found to be in good agreement with those determined from the three- and five-line methods.

However the calculation time is an important factor. In the computation environment in this study, it took 12 steps in 8 s for the three-line method and 40 steps in 33 s for the five-line method to converge. This difference is significant in pixel-based data processing. This justifies the minimal run of the self-consistent five-line method to determine rough values of L_p as the input value for the three-line method.

4. Discussion and Summary

The L_q in the five-line method and those in the $3^1P/4^1P$ method, are compared in Fig. 4, and the difference was found to be a factor of 7. The constrain of the $n(501;\ 3^1P)/n(396;\ 4^1P)$ ratio was recognized to be strong in the determination of L_q. Figure 5 shows the "synthesized" n_e and T_e for different assumptions of L_q. T_e determination using the five-line method was found to be sensitive to L_q, while that using the three-line method was less sensitive. The five-line method with L_q determined from the $3^1P/4^1P$ method (L_probe) provided n_e and T_e that were agreed well with those measured from the probe characteristics. The constraint in the five-line method was not only cast to L_q, but also to T_e. This may be the reason for the discrepancy in Fig. 4. In addition, three-line method also provide the similar values if rough values of L_q is assumed. A difference of about 1 eV is considered to be insignificant in ordinary cases. However, it is important to note that, the transition from the ionizing to recombining plasmas takes place below a few eV in a narrow spatial area and have important effects on the recycling and heat load properties.

To summarize, an improved technique of imaging spectrometry for divertor-relevant low-temperature plasmas using a wavelength-tunable Lyot filter spectral camera was proposed in this paper. The influence of the radiation-trapping effect, characterized by the trapping radius, L_q, can be mitigated using only the triplet series: 471(4^3S), 587(3^3D), and 706(3^3S) nm lines that are in the tunable range of the present Lyot filter. Approximate values of L_q can be determined by adding 501(3^1P)- and 667(3^1D)-nm singlet lines.

These lines were free from the leak-bands of the Lyot filter. More active elimination of leak-bands has been achieved by combining red–green–blue filters [12] or using a color CCD detector [4].

Acknowledgments

The experiments in this work were conducted as a part of the master's thesis of A. Muraki supervised by the author (Univ. Tokyo, 2009-2011). The author acknowledges Y. Iida (Bunkokeiki Co., Ltd.) for valuable discussion on radiation trapping. This work was partially supported by JSPS KAKENHI Grant Numbers 21540507 and 16K05631.

[1] B. Schweer, G. Mank, A. Pospieszczyk *et al.*, J. Nucl. Mater. **196-198**, 174 (1992).
[2] M. Goto, J. Quant. Spectrosc. Radiat. Transf. **76**, 331 (2003).
[3] S. Kado, H. Suzuki, Y. Kuwahara *et al.*, Plasma Fusion Res. **2**, S1125 (2007).
[4] M. Yamano, S. Kado, S. Kushita *et al.*, JPS Conf. Proc. **1,** 015015 (2014).
[5] S. Kado, Y. Iida, S. Kajita *et al.*, J. Plasma Fusion Res. **81**, 810 (2005).
[6] S. Kado, M. Goto, K. Sawada *et al.*, J. Plasma Fusion Res. **86**, 631 (2010) [in Japanese].
[7] Y. Iida, S. Kado and S. Tanaka, Phys. Plasmas **17**, 12, 123301 (2010).
[8] Y. Iida, S. Kado, A. Okamoto *et al.*, J. Plasma Fusion Res. SERIES **7**, 123 (2006).
[9] K. Sawada *et al.*, Plasma Fusion Res. **5**, 001 (2010).
[10] S. Kajita and N. Ohno, Rev. Sci. Instrum. **82**, 2 (2011).
[11] Y. Kuwahara, M. D. Thesis, The University of Tokyo (2008) [in Japanese].
[12] S. Abe, M. D. Thesis, The University of Tokyo (2012) [in Japanese].